scientific reports

Check for updates

OPEN

The meteorological drivers of mass coral bleaching on the central Great Barrier Reef during the 2022 La Niña

Lara Shania Richards[1,2,3]✉, Steven Thomas Siems[1,2,3], Yi Huang[2,3,4], Wenhui Zhao[2,4], Daniel Patrick Harrison[2,5], Michael John Manton[1] & Michael John Reeder[1,3]

The frequencies of marine heatwaves and thermal coral bleaching events (CBEs) over the Great Barrier Reef (GBR) continue to increase with five mass CBEs reported since 2016. While changes in the local meteorology, such as reduced wind speeds and decreased cloud cover, are known to heat the shallow reef waters, little consideration has been given to the overriding synoptic meteorology. The 2022 CBE, occurring under La Niña conditions, saw ocean temperatures at Davies Reef increase 1.9 °C over 19-days and subsequently cool 2.1 °C back to seasonal norms over eight days. This event was found to be triggered by repeated Rossby wave breaking disrupting the local trade winds, thus inhibiting the latent heat flux. Latent heat fluxes, the primary driver of the event, tripled as the trade winds returned via rapid coastal ridging. These same synoptic features are concurrent with the historic Lismore flooding located hundreds of kilometres south of the GBR.

Keywords Coral bleaching, Trade winds, Marine heatwave, Great Barrier Reef

The Great Barrier Reef (GBR) is the world's largest coral reef, extending from the subtropics (24°S) to the deep tropics (10°S). This UNESCO World Heritage site, renowned for its biodiversity, has been classified as "under threat" with one of the greatest dangers arising from mass thermal coral bleaching events (CBEs), which occur during localised marine heatwaves (MHWs). Since 1998, eight mass thermal CBEs have occurred on the GBR, with five of them since 2016[1]. The 2022 CBE was particularly widespread with damage to 91% of the reefs surveyed[2]. This event has garnered further interest as it occurred during the 2021–2022 La Niña, which is "a climate state historically associated with increased cloud cover, rainfall and cooler summer water temperatures" along the GBR[3]. However, Spady et al.[4] noted 'unprecedented' early-summer heat stress along the extent of the GBR prior to the event, highlighting the unusual climatic antecedent conditions.

Mass thermal CBEs result from a combination of elevated ocean temperatures and high solar radiation levels, including ultraviolet radiation, leaving the coral visibly bleached[5–7]. In the shallow waters of a coral reef, connections between the local meteorology and thermal CBEs have been reported since the 1960s[8]. These connections can occur on the time scale of days to weeks and have been studied across coral reefs globally[9–11], including the GBR[3,12–15]. In recent decades, Skirving et al.[12], Bainbridge[16] and Karnauskas[14] emphasized the connection between light local winds and the increase in near-surface ocean temperatures. Such periods of light winds commonly coincide with clear skies, high humidity, and higher air temperatures, providing ideal conditions for coral bleaching[10,11,13,17]. The local cloud cover regulates the radiative fluxes (short-wave and longwave), while surface winds, air temperature, and relative humidity modulates the turbulent fluxes (sensible and latent heat) across the ocean surface. During periods of clear skies and weak winds, these compound effects dampen many of the ocean's cooling mechanisms, allowing ocean temperatures in a shallow reef environment to rise quickly[15,18], often becoming MHWs[19].

The meteorology over the GBR is commonly characterised by the trade winds, which are persistent south-easterly surface winds with an upper-level inversion typically between 1.5–2.5 km, capping the height of trade cumulus convection[20–22]. Across the GBR, the trade winds are strongest in austral winter when the subtropical

[1]School of Earth, Atmosphere and Environment, Monash University, Clayton 3800, Australia. [2]Reef Restoration and Adaptation Program, Coffs Harbour, Australia. [3]The ARC Centre of Excellence for Climate Extremes, Melbourne, Australia. [4]School of Geography, Earth and Atmospheric Science, The University of Melbourne, Melbourne 3010, Australia. [5]National Marine Science Centre, Southern Cross University, Coffs Harbour 2450, Australia. ✉email: Lara.Richards@monash.edu

ridge and intertropical convergence zone (ITCZ) are located furthest north. As austral summer approaches, the subtropical ridge and ITCZ shift southwards, and the Australian monsoon begins to dominate northern Australia, including parts of the GBR[20,23,24]. During summer, when the trade winds along the GBR are weakest and tropical convection is strongest, disruptions to these trade winds are more frequent[21,23,24].

Although the GBR ocean temperatures have been unseasonably high since December 2021, coral bleaching was reported in 2022 and most recently in 2024, but not 2023. The 2022 CBE, the subject of this research, was the result of a MHW that developed largely across the central GBR[2]. At Davies Reef, located in the central GBR (Fig. 1), the 4 m ocean temperature (T_{4m}) increased from 28.6 °C to 30.5 °C over a 19-day period (February 20th–March 10th 2022). Rapid cooling soon followed with temperatures falling 1 °C in 48 h and shortly back to seasonal norms (28.3 °C) over the next week. During this event, the T_{4m} at Davies Reef met the criteria for a MHW[25] from February 26th–March 15th. Concurrent with this CBE, widespread flooding was recorded across regions to the south of the GBR, spanning Brisbane (Queensland) to Lismore (New South Wales) (Fig. 1). Flooding at the town of Lismore, located approximately 1250 km south of Davies Reef, was recorded from February 22nd–March 9th with peak flood level exceeding the historic record by more than two meters[26]. The overlapping timing of these two extreme events in the same region prompts a more comprehensive understanding of the synoptic meteorology and the linkage between the two extremes.

Many previous studies of GBR CBEs have focused on multiple events and/or time scales of a month or longer[3,13,14], providing a strong foundation for understanding the background climate. At such time scales, however, these studies are unable to unravel the response of the GBR ocean temperatures to the synoptic meteorology. Thus, in this study, we present an analysis of the local and synoptic meteorological evolution during the 2022 CBE and accompanying MHW focused on Davies Reef during February–March 2022. While coral bleaching is a multifaceted process, we aim here to understand the role of the local and synoptic meteorology in driving ocean temperatures during the 2022 GBR CBE. Using local observations from Davies Reef, satellite imagery from the Himawari-8 Advanced Himawari Imager (AHI) and thermodynamic and radiative fields from the European Centre for Medium-Range Weather Forecasts (ERA5) reanalysis, a surface energy budget is constructed at this central location. Through the energy budget the role of the meteorology is explored throughout the onset, amplification, and recovery of the CBE. Building from the local meteorology, the synoptic meteorology is analysed revealing a wide-spread breakdown of the trade winds over this period and the direct connection to the Lismore floods.

Materials and methods

Data

The case study of the 2022 CBE was defined for the Australian Institute of Marine Science's (AIMS) Davies Reef (18.83 °S, 147.63 °E) automatic weather station (AWS), located 100 km northeast of Townsville in the central GBR (Fig. 1). Despite the widespread coral bleaching reported across the GBR in 2022, Davies Reef was chosen due to its long observational record dating back to 1991. The Davies Reef AWS, located on a 12 m platform, collects observations of ocean temperatures at 4 m (T_{4m}), 8.5 m ($T_{8.5m}$), and 18.5 m ($T_{18.5m}$), air temperature (T_{air}), relative humidity (RH), rainfall accumulation, wind speed and wind direction all at 10-min intervals. Daily averages of the T_{4m} dataset are extended back to 1996 to cover the eight recent GBR CBEs, noting that observations from April 23rd–30th 2024 were unavailable and therefore omitted from all analysis. Missing data are filled by interpolating the T_{2m} and T_{8m} records (0.59% of data), while for the rare occasions when this interpolation over depth was not possible, the daily T_{4m} was estimated by averaging the daily T_{4m} from the

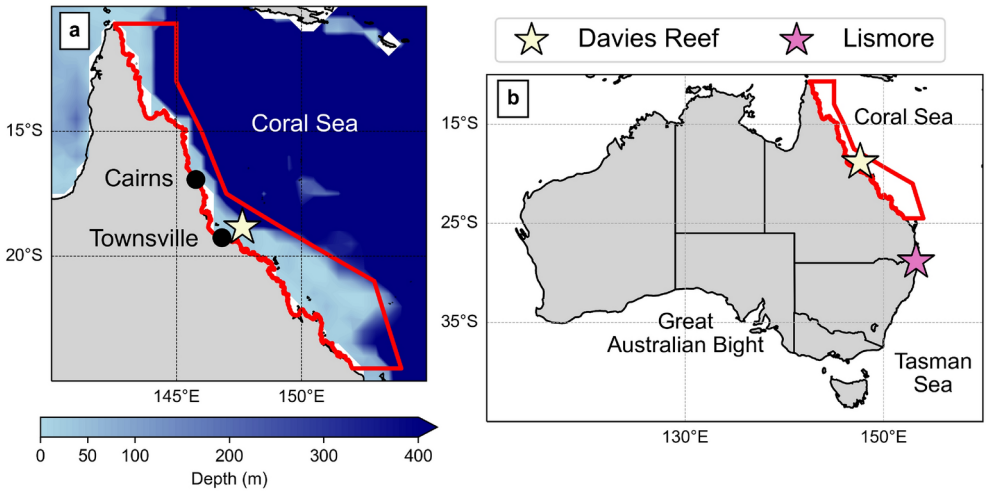

Figure 1. Reference maps of key areas mentioned in this study. Panel (**a**) shows the ERA5 bathymetric map of the GBR region, while panel (**b**) shows the Australian domain. Davies Reef is denoted by the pale yellow star and Lismore by the pink star. The GBR extent is indicated by the red outline in both panels. Both panels were generated using Python 3.9.6 (http://www.python.org) including matplotlib 3.7.1 and Cartopy 0.21.1.

nearest available days (0.07% of data). The closest tide gauge to Davies Reef (Townsville) is used to analyse tidal ranges for the study period[27]. However, we note the potential uncertainty of tidal variation over the shallow reef in the absence of on-site tide gauges.

It is important to acknowledge that due to that given the absence of ocean turbulence and atmospheric radiation sensors at Davies Reef, ERA5[28] net flux data alone is used to calculate the net surface energy budget. ERA5 records on hourly intervals with a $0.25^\circ \times 0.25^\circ$ grid-spacing are used to both calculate the net surface energy budget and extend the analysis to the synoptic scale. As ERA5 surface values were found to be highly consistent with the AIMS platform observations ($r > 0.8$), vertical profiles of ERA5 air temperature, relative humidity, and horizontal winds are taken at the closest grid point to Davies Reef to produce 0000 UTC (1000 LST) atmospheric soundings.

The net surface energy budget at Davies Reef is calculated using ERA5 daily averaged mean net surface fluxes at the closest grid point to Davies Reef, where the contribution of each flux, short-wave (Q_{SW}), longwave (Q_{LW}), sensible (Q_H), and latent heat (Q_E), to the total net flux (Q^*) is calculated (Eq. 1).

$$Q^* = Q_{SW} + Q_{LW} + Q_H + Q_E. \tag{1}$$

Here, a positive (negative) flux represents downwelling (outgoing) energy. ERA5 is commonly used in replacement of in-situ flux measurements[14,29] and is highly comparable to the outputs of other combined reanalysis and observational products (INCOIS TropFlux version 1 and WHOI Objectively Analysed Air-Sea Fluxes version 3)[14]. The ocean advection terms were excluded from this calculation as on a short time scale, their impact is insignificant over the GBR in comparison to the other terms[14].

Daily 0000 UTC (1000 LST) ERA5 horizontal winds, mean sea-level pressure (surface), and geopotential height (500 hPa and 250 hPa) data are used to illustrate the synoptic meteorology. Lastly, the local fractional cloud cover (daytime only) is calculated from the Himawari-8/AHI satellite (2 km resolution on 10 min intervals) using level-2 cloud mask data over a $1^\circ \times 1^\circ$ domain centred on Davies Reef.

Climatological analysis and event definition

Ocean temperatures are commonly seen as the most reliable proxy for CBEs, where the use of ocean temperature thresholds in bleaching curves (see Berkelmans[30]) can indicate periods of high coral stress and potential bleaching[30,31]. As bleaching curves and associated temperature thresholds are calculated using daily averaged ocean temperatures, accordingly, the daily averaged T_{4m} is used to identify the 2022 coral bleaching period at Davies Reef. The analysis is then extended to austral summer and the GBR coral bleaching season (December–April)[15] from 1996–2024 to compare the recent eight GBR CBEs.

From Fig. 2, the Davies Reef T_{4m} exceeds 30 °C on two occasions over the 2022 summer, with the second period in February–March aligning with the March bleaching reports. The GBR cools between these two heating spikes with T_{4m} dropping below the climatological mean in early February. Typical methods for analysing CBEs include local bleaching thresholds and bleaching curves[30], degree heating weeks[32] or by defining a MHW event[25]. While these methods have proven useful in identifying the CBEs peak and comparing event intensity, they can miss significant details behind the onset and collapse of individual events. For example, when using a 7-day running mean, the local bleaching threshold at Davies Reef is calculated to be 29.8 °C[30], making the 2022 coral bleaching period March 2nd–12th 2022. While under the MHW definition presented by Hobday et al.[25], the bleaching period is between February 26th–March 15th 2022. These methods do not capture the entire period of heating and cooling associated with this CBE (Fig. 2). Instead, we define the start of the 2022 CBE by working backwards from the MHW start (February 26th) and finding the first day the period averaged daily $dT_{4m}/dt < 0.1$ °Cday^{-1}, which is February 20th. Similarly, we define the end of the CBE by working forwards from the MHW end (March 15th) and finding the first day at which the period average daily $dT_{4m}/dt > -0.15$ °Cday^{-1}

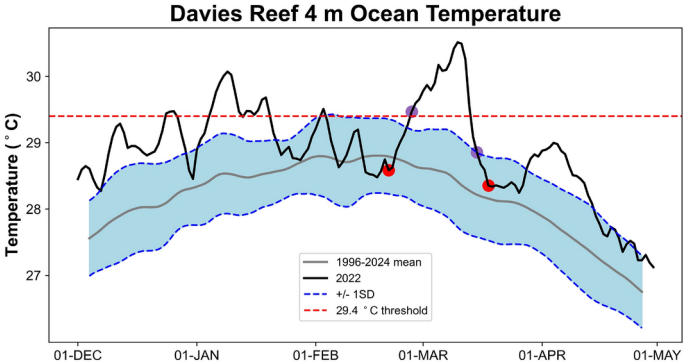

Figure 2. AIMS 2022 4 m ocean temperature at Davies Reef (black) compared to the 1996–2024 7-day moving mean (grey) and ±1SD for the December–April period (blue dashed) with the 29.4 °C threshold (red dashed). Red dots indicate the 2022 CBE start and end dates, while purple dots show the MHW start and end dates.

, which is March 18th. We then split the CBE into a heating and cooling period using the date of the maximum daily average temperature (March 10th) to separate the two periods.

Next, in order to compare 2022 with recent CBEs, similar to the MHW definition, a curve of one standard deviation (+1SD) above the climatological mean T_{4m} can be calculated (Fig. 2), which peaks at 29.4 °C in February. Here we use both the +1SD curve and a fixed threshold of 29.4 °C to analyse the eight recent mass CBEs, noting that the 2006 CBE was limited to the southern GBR and not observed at Davies Reef. Furthermore, the 'degree heating days', i.e., exposure time × degrees above threshold[30], can readily be calculated for both thresholds, providing a measure of the cumulative intensity of T_{4m} for each bleaching season (Fig. 3). Note the lower threshold of 29.4 °C was used in place of the 29.8 °C local bleaching threshold for the degree heating days analysis as the 29.8 °C threshold removes the majority of the cumulative intensity, making event comparison difficult.

Results

Event comparison

Comparison between the 2022 CBE and the other seven recent CBEs shows that 2022 was an anomalously warm year at Davies Reef, with the highest number of days exceeding both thresholds for the analysed period (Fig. 3). The CBEs outside of 2022 had an average degree heating days value of 11.5 °C (13.1 °C excluding 2006), while the degree heating days value for 2022 was roughly four times larger at 39.8 °C for the +1SD threshold (Fig. 3a). However, a comparison of the number of days and degree heating days above the 29.4 °C threshold shows the peaks of the 2022 and 2020 events are similar, with 2024 closely behind (Fig. 3b). This indicates that the large value of the +1SD degree heating days for 2022 was the result of a warm December–January outside of the reported bleaching period (Fig. 2). Thus, the significant temperature spike, occurring in an anomalously warm year, combined to produced the high cumulative intensity at Davies Reef during the 2022 CBE, even though T_{4m} had cooled to below the climatological mean prior to the onset of the event in mid-February.

Local analysis

Having used T_{4m} to locally define the 2022 CBE at Davies Reef (February 20th–March 18th), the local ERA5 surface energy budget is constructed at the daily time scale. From this, using further observations from the AIMS Davies Reef AWS, and Himawari-8/AHI satellite, we now explore the relationship between the near-surface ocean temperature and the ocean heating forced by the local meteorology (Figs. 4, 5).

Giving first a broad overview, both daily averages of T_{4m} and $T_{8.5m}$ rise in close unison from 28.6 °C to 30.5 °C over 19-days during the heating period. While differences between the T_{4m} and $T_{8.5m}$ daily maximums are largest between February 22nd–28th (0.4–0.5 °C) indicating a weakening in wind-driven ocean mixing, the overall correlation between their 10-min observations during the heating period (0.989) and across the 2022 CBE (0.984) is remarkably high. This strong correlation indicates that the ocean mixed layer extended to at least 8.5 m during the heating period (Fig. 4a). We do also note as wind speeds increase, this maximum temperature difference decreases, indicating their good correlation (−0.69). During the subsequent cooling period, ocean temperatures fall rapidly to 28.4 °C in only eight days, where the average temperature change is roughly twice as strong as the warming period (Table 1). The daily average T_{4m} and $T_{8.5m}$ are strongly correlated throughout the study period (0.996), while $T_{18.5m}$ decouples from the upper layers around March 7th, plateauing at 30 °C (Fig. 4a). As expected the surface Q^* remains strongly positive during the heating period, switching rapidly to negative during the cooling period.

Prior to the onset of the event, the surface winds are typical trade winds being relatively strong and south-easterly, ranging from 8–12 ms^{-1}. The daytime cloud fraction averages 80%, where during this time, the T_{air} is relatively cool at 27–28 °C, and the *RH* is at 75–80%. These conditions are consistent with the climatological trade wind conditions at this time of year (Table 1). In the early days of the heating period, February 20th–24th , the trade south-easterlies begin to weaken, forcing a significant reduction in Q_E and Q_H by 75 Wm^{-2} and 19 Wm^{-2} respectively. The average cloud fraction falls to ∼60% as the daily rainfall weakens and Q_{SW} slowly increases. The large reductions in the turbulent fluxes result in Q^* increasing to 127 Wm^{-2} indicating a net heat flux into the ocean. Ocean temperatures at all three depths rise at this time noting the T_{4m} daily maximum is roughly 0.4–0.5 °C above the $T_{8.5m}$ maximum. Throughout February 25th–28th, the winds continue to weaken reaching a minimum of 1.8 ms^{-1} with the direction reversing to northerly. The trade winds have completely collapsed, while ocean temperatures at all depths continue to increase as the MHW period starts on the 26th. The change to light northerly winds and absent rainfall allows the heat and humidity to build in the boundary layer. Surface *RH* increases to ∼80% and T_{air} reaches 29 °C, while Q_E falls to a minimum of −52 Wm^{-2}. A minimum cloud fraction (33%) sees Q_{SW} peak at 298 Wm^{-2}, presumably close to the clear-sky maximum, as Q^* reaches 190 Wm^{-2}, the highest recorded in the entire study period.

Between March 1st–7th, the northerly winds increases to ∼9 ms^{-1} bringing warm (T_{air} 29–30 °C) and moist (80–83% *RH*) air to Davies Reef, only slightly cooler than the ocean at T_{4m}. Ocean temperatures at all depths continue to increase before briefly plateauing at 30 °C. Q^* decreases to 110 Wm^{-2}, as Q_E increases in response to the higher wind speeds. However, the high *RH* limits evaporation at the surface, preventing Q_E from reaching larger values common under trade wind conditions. The cloud fraction remains relatively low (36–64%), keeping Q_{SW} close to the clear-sky maximum while rainfall is largely absent. As the northerly winds again weaken between March 7th–10th, both T_{4m} and $T_{8.5m}$ reach their peak at 30.5 °C, while the $T_{18.5m}$ stabilises at 30 °C. The combination of warm air and calm winds promote weak turbulent fluxes as Q_H is negligible at −0.4 Wm^{-2} and Q_E averages −81 Wm^{-2}, despite the *RH* falling below 80%. With the cloud fraction remaining low (∼50%), and Q_{SW} remaining high (∼266 Wm^{-2}), the reduction in turbulent fluxes facilitates a strong net heat flux (Q^*) into the ocean (∼136 Wm^{-2}).

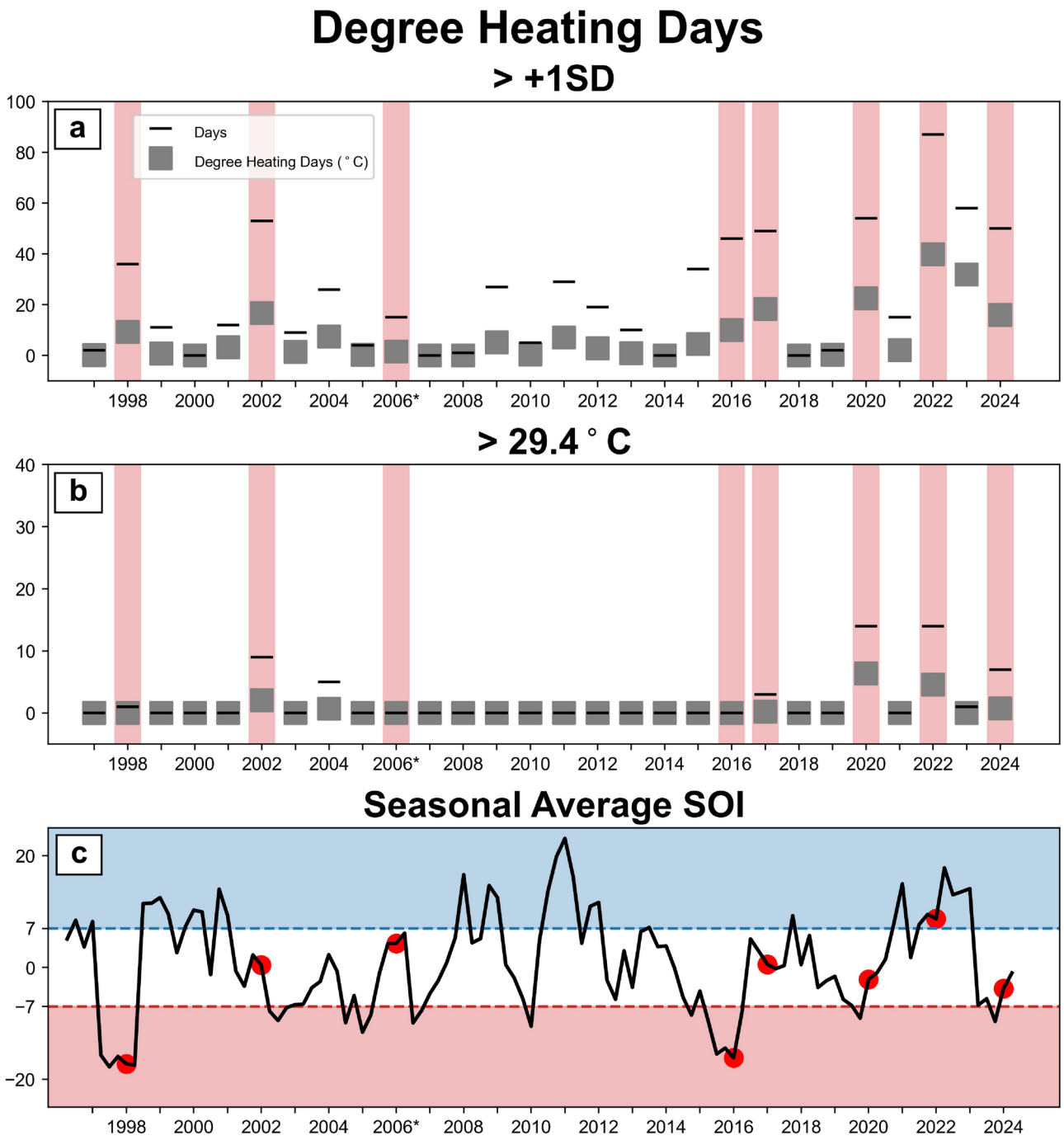

Figure 3. Event comparison during the 1996–2024 December–April periods. Coral bleaching years are indicated in red. The area between the Davies Reef T_{4m} daily average ocean temperature and the +1SD curve (**a**) and above 29.4 °C (**b**) are shown by the squares (degree heating days), while the number of days represented by the horizontal line. It is important to note that the event comparison used in this study is location specific to Davies Reef. Thus, as 2006 (southern GBR localised bleaching) is the only reported bleaching year not to influence the central GBR (or Davies Reef), its true intensity will not be present in this analysis. Data was not available for T_{4m} during April 23rd–30th 2024, which may have a small impact on the +1SD value but not the 29.4 °C threshold. Panel (**c**) shows the Bureau of Meteorology seasonally averaged Southern Oscillation Index (SOI) for 1996–2024. Red markers indicate the eight GBR CBEs. SOI values >7 indicate La Niña periods and SOI values < -7 indicate El Niño periods.

The transition between heating and cooling periods is marked by a sudden wind shift, increased wind speeds, and rapid ocean cooling at all depths. Between March 10th–11th, the surface winds turn from northerly to easterly, coinciding a drop in T_{air} and RH over a period of hours (not shown). As the wind speeds increase, so do the turbulent fluxes. Combined with a jump in cloud fraction to 80% and subsequent drop in Q_{SW} to 189

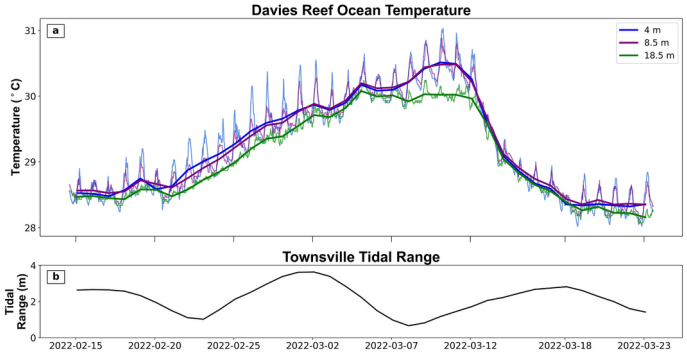

Figure 4. Panel (**a**) shows the AIMS Davies Reef AWS observational ocean temperatures between February 15th-March 23rd 2022. The 4 m (blue), 8.5 m (purple) and 18.5 m (green) ocean temperatures are shown with their daily average (thicker line) and 10-min observations (thinner line) to represent the diurnal cycle. Panel (**b**) shows the daily tidal range observed at the Townsville tide gauge roughly 100 km south-west of Davies Reef.

Wm^{-2}, Q^* falls to 34 Wm^{-2}. The trade winds have been re-established and continue to strengthen throughout the cooling period. From March 11th–13th, T_{4m} drops by a full degree as wind speeds peak at 12 ms^{-1}. Q_E soon peaks at −340 Wm^{-2}, while the cloud fraction approaches 100% bringing heavy rainfall (∼90 mm day^{-1}) on the 13th which severely dampens Q_{SW} as Q^* reduces to ∼−220 Wm^{-2}. By March 15th the MHW period ends and T_{4m} falls below 29 °C. By March 18th, T_{4m} has dropped over 2 °C. Now within the +1SD curve, the period of heat stress ends for the season in this region.

Comparing the average heating/cooling conditions to the February–March average highlights the drastic effects the meteorology had on local ocean temperatures (Table 1). The February–March climatological average meteorology for Davies Reef describes a trade wind regime, where the surface winds are blowing from the east, and the wind speeds are relatively higher at 7.5 ms^{-1}. Q^* is close to zero indicating a balance between the net heating (Q_{SW}) and net cooling terms (Q_E, Q_H and Q_{LW}).

During the heating period, the trade wind structure collapses, resulting in winds that are on average 10% weaker than the mean and blow from the north. The cloud fraction falls to 52% and *RH* increases to 78%. Q^* is strongly positive, with Q_{SW} increasing by 37% (equivalent to 43 Wm^{-2}) and Q_E decreasing by 42% (equivalent to 68 Wm^{-2}) relative to the average. The dT_{4m}/dt change indicates a gradual yet steady heating rate at 0.1° Cday^{-1} for the 19-day period.

During the cooling period, the trade winds re-establish becoming stronger than normal. On average, wind speeds are 33% higher than the mean and the heading changes to east-south-easterly. The RH drops to 72% and the cloud fraction increases to 93%. Q^* turns strongly negative, with a 32% decrease in Q_{SW} (equivalent to 74 Wm^{-2}) and 56% increase in Q_E (equivalent to 89 Wm^{-2}) compared to the mean. The dT_{4m}/dt temperature change is approximately 2.5 times the rate seen in the heating period, at −0.27 °Cday^{-1}, providing the rapid cooling for this period.

Correlations are then analysed for both the entire study period (February 20th–March 18th) revealing a strong relationship (0.81) between dT_{4m}/dt and Q^*. Of the four flux components, the correlation between Q_E and dT_{4m}/dt is strongest at 0.79, indicating a robust linkage, while Q_{SW} and dT_{4m}/dt is slightly weaker at 0.74. Despite this, wind speed, which strongly influences Q_E, shows a more modest correlation (−0.31) suggesting that wind speed alone is not a strong proxy for CBEs. Remarkably, while the correlation between Q_{SW} and cloud fraction is expectedly strong (−0.89), Q_E also boasts a strong correlation with the local cloud fraction (−0.87). While the influence of Q_E on low-level marine clouds is well documented[20,33], it's noteworthy that the Himawari daytime cloud fraction also includes mid to high-level clouds, which should be less responsive to surface fluxes. All correlations, excluding wind speed, were found to be statistically significant with p-values < 0.01.

Atmospheric profile and cloud conditions

Given the critical impact of the trade winds on local ocean temperatures at Davies Reef, the trade wind vertical structure is examined to better understand their evolution and development throughout the 2022 CBE. The trade winds are present at Davies Reef at least five days prior to the start of the heating period, with the trade wind inversion base presenting at ∼650 hPa and the lower-level winds are strong, blowing from the south-east (not shown). Approaching the heating period, there is a noticeable descent and weakening of the inversion layer indicating the trades are starting to break down.

With the onset of the heating period on February 20th, the weakened trade wind structure persists with south-easterlies dominating the lower-levels (Fig. 6a), as the inversion height has lowered to ∼750 hPa. The profile is close to saturation and the daytime cloud fraction at Davies Reef remains high (77%), as shallow cumulus and high clouds extend over the central-southern GBR (Fig. 7a). By February 25th, the trade winds have collapsed (Fig. 6b). Calm winds form up to 900 hPa as a shallow inversion caps the boundary layer. The surface layer is warm and moist, yet above the inversion the upper atmosphere is drying as the dew point temperature decreases by ∼5–10 °C. As the boundary layer warms, convective inhibition (CIN) builds from ∼10 J kg^{-1} to 40 J kg^{-1} and soon to a maximum of 75 J kg^{-1} on February 28th. When coupled with the weak turbulent fluxes, this CIN

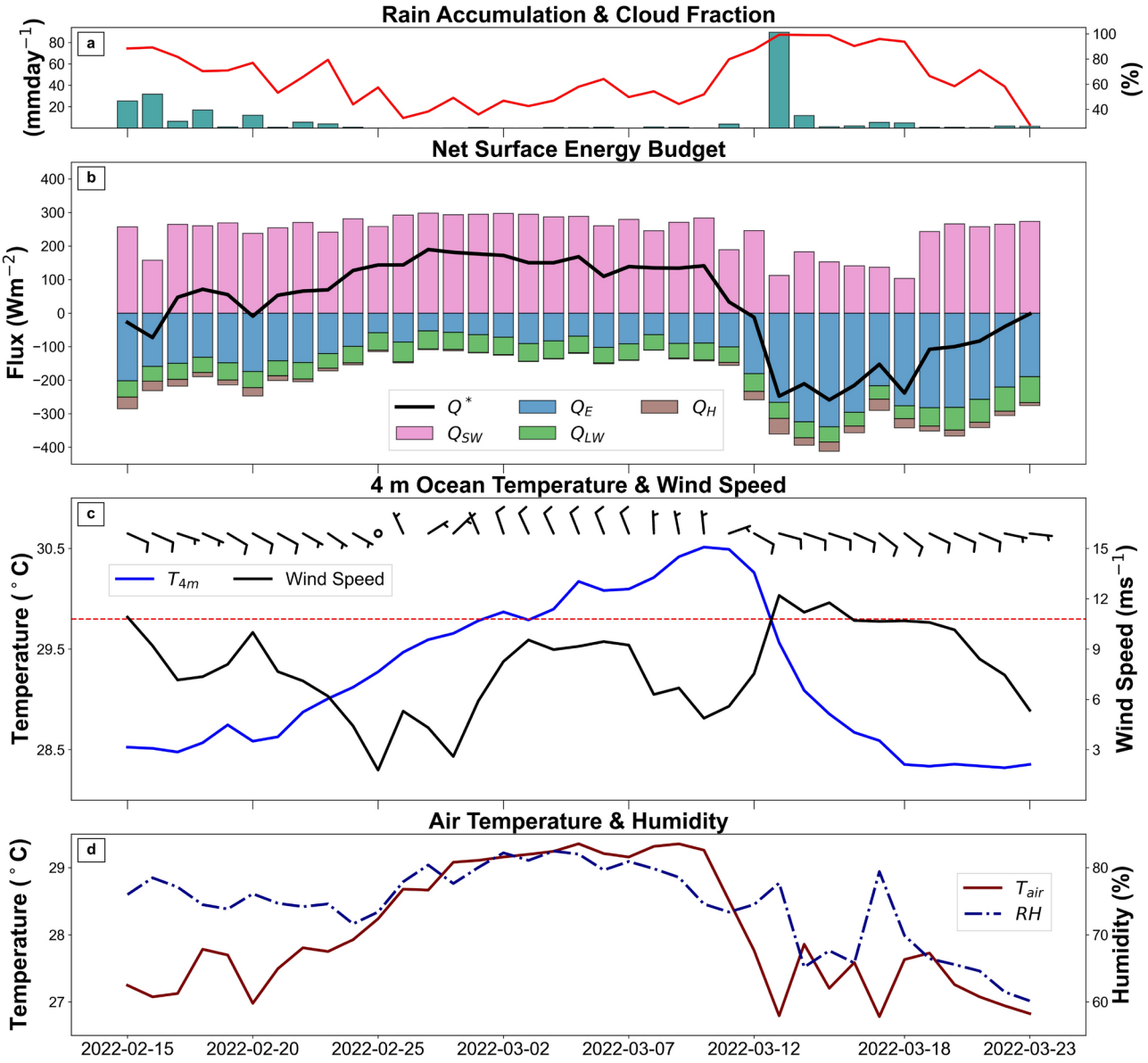

Figure 5. Davies Reef daily averages between February 15th-March 23rd, 2022. Panel (**a**) shows the 1° daytime cloud fraction for Davies Reef using Himawari-8/AHI satellite data and AIMS daily accumulated precipitation. Panel (**b**) shows the ERA5 net surface energy budget. The stacked bar chart shows the individual flux components; short-wave (Q_{SW}, pink), long-wave (Q_{LW}, green), sensible heat (Q_H, brown) and latent heat (Q_E, blue), where positive (negative) values represent incoming (outgoing) flux. Panel (**c**) shows AIMS observational ocean temperature at 4 m (blue) vs AIMS surface wind speed (black) and wind barbs (ms^{-1}) with the 29.8 °C local bleaching threshold (red dashed). Panel (**d**) shows AIMS surface air temperature (maroon) vs surface relative humidity (blue dashed).

prevents any substantial convection through the boundary layer, which remains largely cloud free (57% cloud fraction), as the high cloud cover disappears (Fig. 7b).

The transition from calm winds to strong northerlies is evident on March 4th (Fig. 6c). These northerlies, reaching up to 900 hPa, produce an exceedingly warm and moist boundary layer. Above the boundary layer the atmosphere has further dried. Westerly winds bring dry continental air over the GBR as the daytime cloud fraction, still dominated by shallow cumulus, drops to 47% (Fig. 7c). As the heating period ends on March 10th, the low-level northerlies weaken and dew point temperatures increase above 650 hPa (Fig. 6d). The boundary layer remains warm as only shallow cumulus persist over the central GBR (52% cloud fraction) (Fig. 7d).

With the onset of the cooling period, the re-establishment of the trade winds is evident on March 12th (Fig. 6e). South-easterly trade winds have formed below 500 hPa, while lower-level air temperatures have decreased. The profile is close to saturation below 750 hPa as deep convection pushes over Davies Reef from the south (Fig. 7e), bringing the daytime cloud fraction up to 88%. As the cooling period ends on March 18th,

	Heating	Cooling	FEB–MAR
	(FEB 20th–MAR 10th)	(MAR 11th–18th)	'97-'22 mean
Q^* (Wm^{-2})	128.6	−162.6	6.9
Q_{SW} (Wm^{-2})	275.4	158.2	232.3
Q_{LW} (Wm^{-2})	−49.7	−44.8	−52.2
Q_H (Wm^{-2})	−4.7	−26.2	−12.7
Q_E (Wm^{-2})	−92.4	−249.8	−160.6
WSP (ms^{-1})	6.7	10	7.5
WDR (°)	9.8	110.4	90.2
RH (%)	78	71.7	-
dT_{4m}/dt (°Cday^{-1})	0.1	−0.27	–
1° Cloud Fraction (%)	52.2	93.1	–

Table 1. Heating and cooling period averages compared to the 1997–2022 February–March means. Flux values are calculated with ERA5 daily average net fluxes taken at the closest grid point to Davies Reef (short-wave (Q_{SW}), long-wave (Q_{LW}), sensible heat (Q_H), and latent heat (Q_E) and net flux (Q^*)). Wind speed (*WSP*) and direction (*WDR*) are calculated with AIMS Davies Reef AWS observations. Mean values are not calculated for the 1° cloud fraction or relative humidity (*RH*) as Himawari-8/AHI data is only available from 2015 and *RH* data from 2008.

the trade wind profile persists featuring a pronounced easterly component in the low-level winds (Fig. 6f). The surface layer has experienced a slight cooling and drying, while the atmospheric profile reaches saturation at 500 hPa and upwards of 300 hPa. As deep convection covers the GBR, the daytime cloud fraction remains high at 94% (Fig. 7f).

Synoptic analysis

Having established the significant role of local meteorology in driving ocean temperature variations at Davies Reef, our next goal is to broaden this insight across the GBR. Connecting the synoptic meteorology to the surface observations and atmospheric profiles, we analyse the breakdown and re-establishment of the trade winds at Davies Reef and their connection to the Lismore floods.

As shown on Fig. 8a, one week prior to the onset of the heating (February 13th), a high-pressure system ridges equatorwards along the east coast and the associated winds are trade south-easterlies. The upper-level jet at 250 hPa and 500 hPa analysis shows a large anticyclonic overturning pattern (Fig. 8b,c), denoting anticyclonic Rossby wave breaking (RWB)[34]. The RWB event extends up to the southern GBR producing cyclonic curvature in the 500 hPa and 250 hPa winds. As the wave breaks, an upper-level cut-off low (COL) is produced around 30° S, 150°E, which persists in the region from February 14th–16th (not shown).

By February 18th, a weak surface low develops over the Coral Sea near 15°S, which strengthens with the commencement of the heating period on February 20th (Fig. 8d). This emerging low disrupts the south-easterly trade winds in the deep tropics, creating areas of calm or northerly surface winds north of Davies Reef. However, the trade wind regime remains over the central and southern sections of the Reef. At this time, an upper-level trough lies over the Southern Ocean (Fig. 8e,f) and the flow over Davies Reef turns from southerly to westerly on the 500 hPa and 250 hPa charts. Over the next four days, this trough extends over southern Queensland eventually resulting in a second anticyclonic RWB event and upper-level COL.

The COL, visible in both the 500 hPa and 250 hPa charts on February 25th (Fig. 8h,i), forms slightly north-west of Lismore. To Lismore's east, a cyclonic circulation just north of an anticyclone creates an upper-level dipole that works against the background westerly flow allowing the COL to stay in the region until February 28th. During this time, the surface low over the Coral Sea expands and deepens to cover the entire GBR region (Fig. 8g). The surface winds over the GBR are light and variable, while the upper-level winds remain westerly with cyclonic curvature at 500 hPa (Fig. 8h,i). The cloud cover over the GBR low is heavily reduced, as dry continental air is pushed over the Reef. Just outside of the low, the cloud cover increases showing deep convection and stronger winds (Fig. 7b). The GBR low eventually moves eastward and by March 4th the surface winds across the GBR becomes northerly (Fig. 8j). In the upper-levels, two anticyclonic RWB events are co-occurring. The larger amplitude wave breaks over Lismore producing strong southerly winds along the Australian eastern coast at 500 hPa and 250 hPa, while a COL has formed over the Great Australian Bight (Fig. 8k,l).

Approaching the heating period's end on March 10th, weak surface pressure gradients reside over the GBR producing calm conditions as the upper-level flow becomes increasingly more zonal (Fig. 9a–c). In the higher latitudes, a high-pressure system moves over the Great Australian Bight while the COL which formed over Lismore has strengthened and tracked south to the Tasman Sea producing strong surface southerlies up the east coast. By March 12th, the high-pressure system has shifted eastward and expanded over the Tasman Sea producing a ridge along the east coast that extends across the southern GBR (Fig. 9d). This synoptic feature is known as 'coastal ridging'[35], being caused by coastally trapped Kelvin waves on the east side of the Great Dividing Range. Strong pressure gradients advance up the east coast to the southern GBR, re-establishing

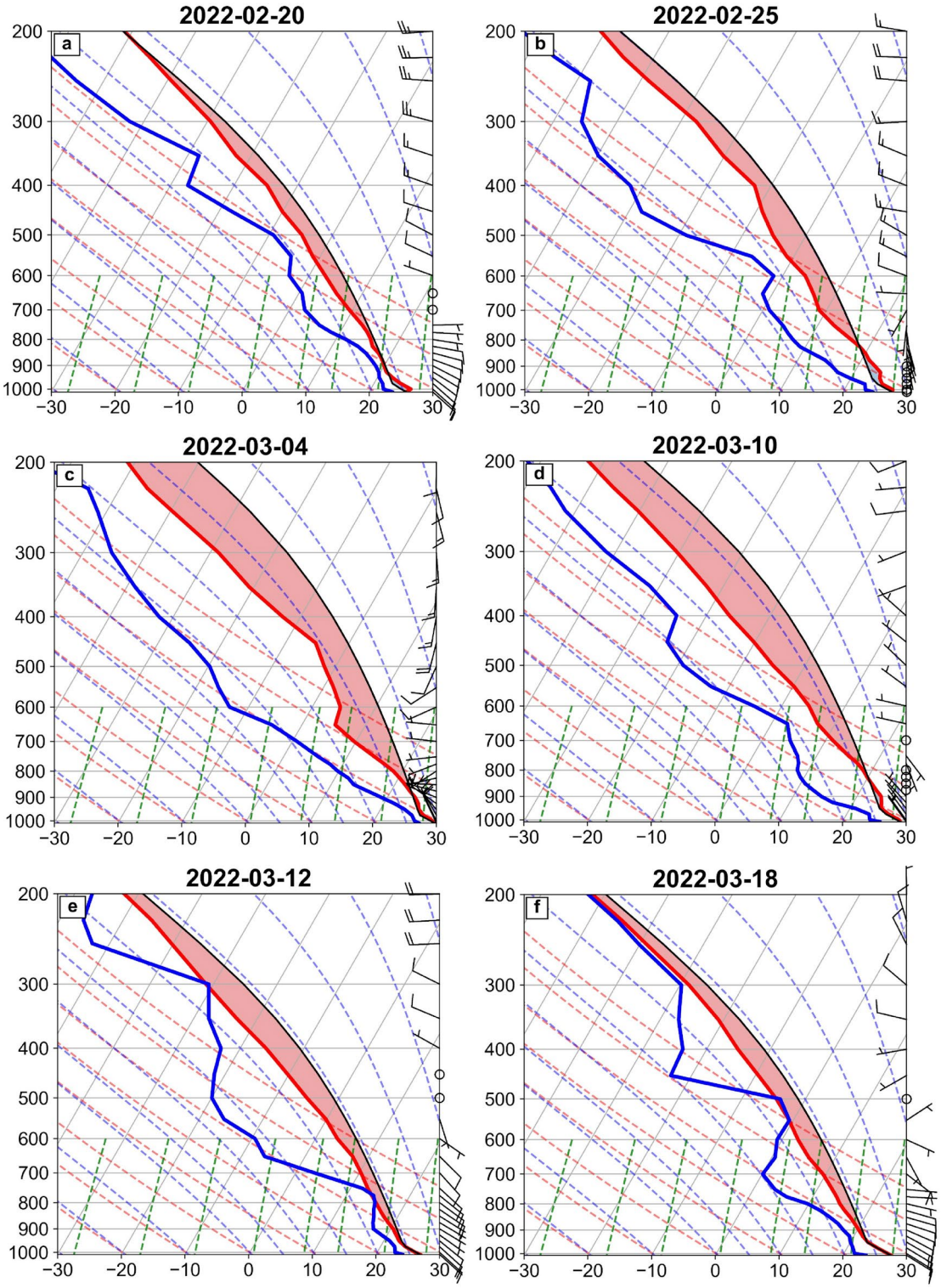

Figure 6. ERA5 atmospheric soundings taken at 0000 UTC (1000 LST) using the closest grid point to Davies Reef. Red lines show air temperature (°C), while the blue lines show dew point temperature (°C). The black line represents the parcel trajectory when lifted from the surface indicating convective available potential energy (red shaded) and convective inhibition (blue shaded) values for the profile.

the south-easterly trade winds over a matter of hours through a front-like wind shift. The upper-level charts (Fig. 9e,f) show a zonal flow, indicating the absence of any RWB. The trade winds continue beyond March 18th (Fig. 9g–i), which marks the end of the cooling period.

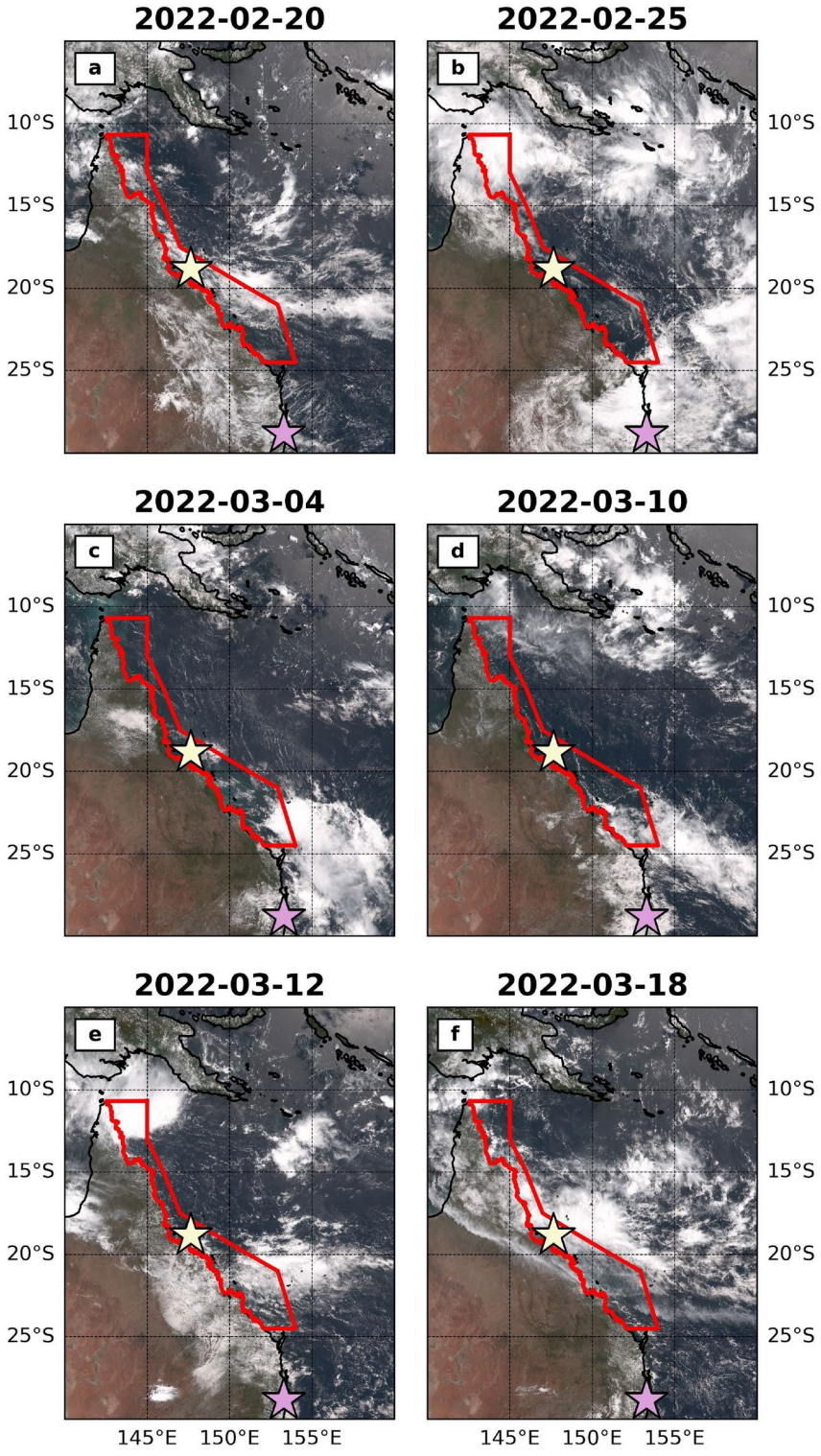

Figure 7. Himawari-8/AHI true colour satellite imagery at 0000 UTC (1000 LST) supplied by the P-Tree System, Japan Aerospace Exploration Agency (JAXA) (https://www.eorc.jaxa.jp/ptree/). The GBR region is outlined in red, while Davies Reef is represented by the pale yellow star and Lismore by the pink star.

The breakdown of the trade winds and the subsequent start of the 2022 heating period at Davies Reef are directly linked to anticyclonic RWB. Repeated RWB events prevented the re-establishment of the trade winds while simultaneously causing flooding over the Lismore region. In the absence of RWB, coastal ridging quickly re-established the south-easterly trades, which cooled the waters of the GBR and thus ending the MHW and the 2022 CBE.

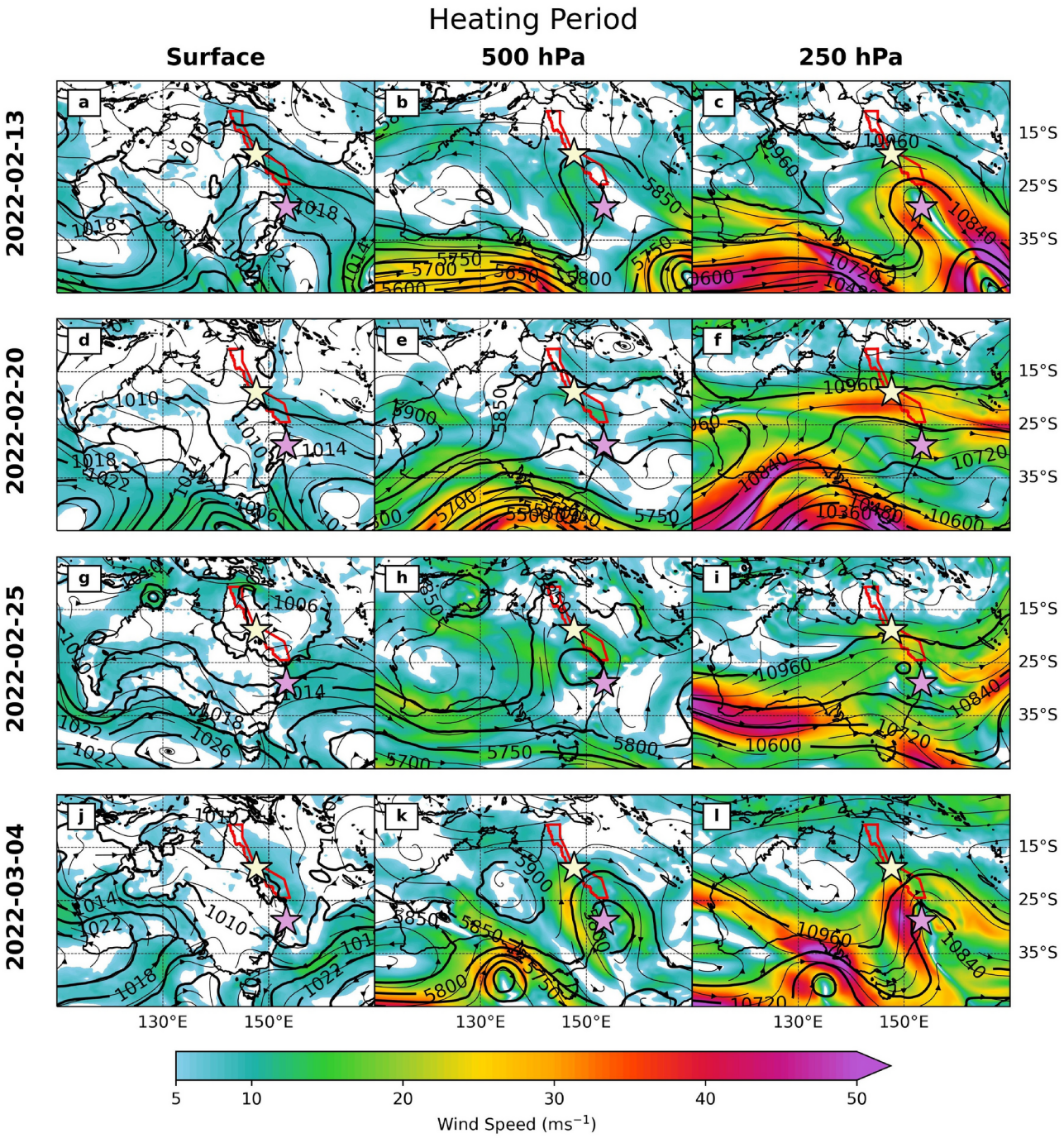

Figure 8. Heating period showing February 13th–March 4th 2022, at the surface, 500 hPa and 250 hPa. All panels are derived from ERA5 data showing wind speed and wind streamlines at each level with pressure (4 hPa intervals) contours at the surface and height contours at 500 hPa (50 m intervals) and 250 hPa (120 m intervals). Pale yellow star represents Davies Reef and pink star represents the location of the 2022 severe floods (Lismore, New South Wales).

Discussion

The influence of the latent heat flux

The disruption and re-establishment of the trade winds impacted all four flux components throughout the 2022 CBE. However, the variation in Q_E was the largest driver of Q^* in both the heating and cooling periods. The phase change from liquid to gas, known as evaporative cooling through the release of Q_E, is the near-surface ocean's strongest cooling mechanism in the absence of clouds[18]. Q_E is a function of both surface wind speed and air-sea humidity differences. Thus, as the trade winds collapse, the subsequent weak winds and high humidity

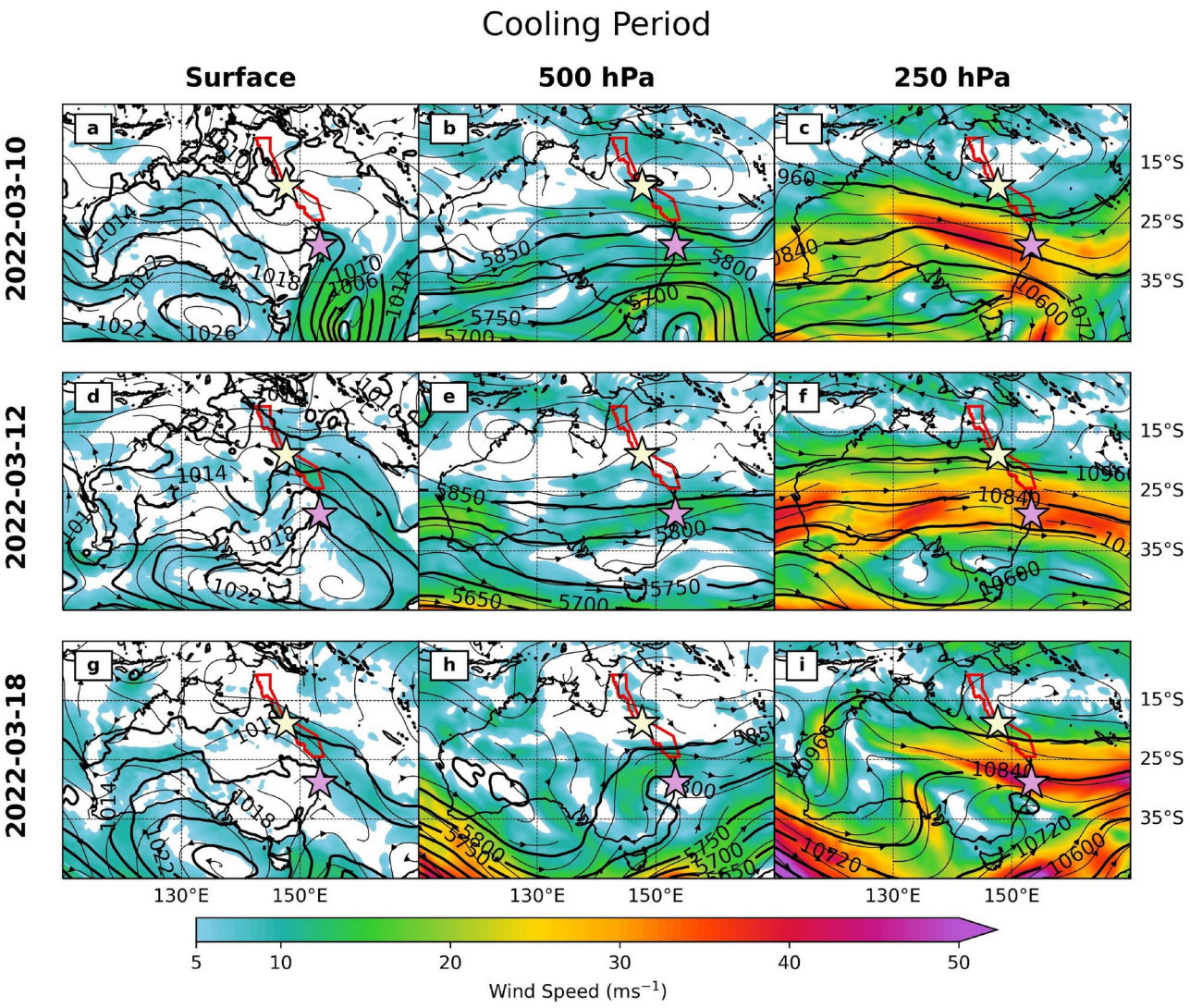

Figure 9. Same as Fig. 8, but showing the cooling period from March 10th–18th 2022.

reduced Q_E by 42% (Table 1), severely limiting the oceans' cooling ability, allowing for the build-up of ocean heat to depths of at least 18.5 m.

Previous studies have mainly focused on surface wind speeds, arguing that the build-up of ocean heat seen in CBEs results from a combination of reduced Q_E and limited ocean mixing from wind-driven ocean turbulence[12,14]. While we do observe the largest difference between the daily maximum T_{4m} and $T_{8.5m}$ when wind speeds are weak (∼0.4 °C), this study has shown only a moderate correlation between wind speed and near-surface ocean temperatures at Davies Reef, likely due to *RH* being overlooked, which can dampen Q_E values even as wind speeds increase. Indeed, from March 1st–7th during the 2022 CBE surface wind speeds increased to 8–9 ms^{-1} on average, similar to those observed under trade wind conditions, yet Q_E remained ∼ 80 Wm^{-2} below the climatological average (Table 1). The transition to northerly winds from March 1st–7th corresponded to a surface humidity jump of over 80% as warm and moist air from the tropics pushes south over the GBR, limiting Q_E even as wind speeds increase. Periods of calm and/or northerly winds with high humidity have been documented over the GBR during ocean temperature spikes[3,13,36], while periods of weak winds and high humidity have also been observed on the Arabian Peninsula to produce ocean temperature spikes[37] and coral bleaching[11,38] due to large reductions in Q_E. Thus, it is necessary to consider both wind speed and humidity to understand the predictability of ocean temperature spikes.

As surface wind speeds increase, so does the surface stress, thus increasing mixing in the near-surface ocean. Higher rates of wind-driven ocean mixing have the potential to reduce near-surface ocean temperatures through the incorporation of the cooler bottom water into the mixed layer. In the absence of wind-driven mixing, the depth of the mixed layer decreases causing the upper-level ocean temperatures to spike as the surface heating is distributed through a shallower layer[12]. Upon initial inspection of Fig. 4a, the T_{4m} and $T_{8.5m}$ are well correlated (0.996) throughout the 2022 CBE, indicating the presence of ocean mixing to at least 8.5 m. However, vertical ocean mixing weakens twice during the study period. From February 22nd–28th, the difference between the

daily maximum T_{4m} and $T_{8.5m}$ is largest, and from March 7th–12th, $T_{18.5m}$ plateaus at 30 °C, while T_{4m} and $T_{8.5m}$ continue to increase. The calm winds during February 22nd–28th likely contributed to a decrease in wind-driven ocean mixing, however the same cannot be said for March 7th–12th. A possible explanation could be a reduction in tidal mixing. Throughout the 2022 CBE, tidal range minimums are found on March 8th (0.7 m) and February 23rd (1 m) (Fig. 4b). The lack of tidal mixing during this period could increase upper-ocean stratification, allowing $T_{18.5m}$ to decouple from the upper layers. As stronger ocean mixing, either tidal or wind-driven, can reduce near-surface ocean temperatures[12,17,19,36,39], further investigation of the impact of tidal ranges during GBR CBEs is needed.

Synoptic dynamics—connection to the mid-latitudes

Given the trades winds influence on near-surface ocean temperatures in the GBR, understanding the initial collapse and subsequent reintroduction of these trades is important. During the 2022 CBE, the trade wind breakdown involves the gradual lowering of the trade inversion as the surface winds weaken at Davies Reef. From the synoptic view, the trade collapse occurs as a low-pressure system forms over the northern GBR between February 13th and 20th, eventually expanding over the entire GBR, displacing the south-easterly trades with calm winds. The initial formation of this low-pressure area is likely explained by the anticyclonic RWB noted on February 13th (Fig. 8c). As the upper-level jet overturns, the associated potential vorticity gradients weaken through mixing, thus weakening the background winds[40,41]. Wave breaking often results in the formation of COLs, which can produce heavy rainfall and flooding on the Australian east coast[41–43], while in the North Atlantic trade wind region, anticyclonic RWB was found to modulate the properties of shallow marine cumulus[44].

Anticyclonic RWB was noted on three occasions throughout the 2022 CBE (February 13th, February 22nd, and March 4th), each forming an upper-level COL. The slow-moving COL on February 22nd, forming just south of the GBR, produced heavy rainfall and flooding across the north-eastern New South Wales region[43]. This COL, combined with a chain of low-pressure systems over the Coral Sea, pulled moisture from the tropics, around the GBR and into the Lismore region[26]. At the same time, westerly winds from the COL moved dry continental air over the GBR, while the boundary layer remained warm and moist due to the surface northerlies. While these dry westerlies could contribute to the clear conditions over the GBR, the low cloud fraction throughout the heating period can also be traced back to the collapse of the trade winds. The trade wind collapse created an increasingly warm and stable atmospheric boundary layer as seen by the increase in CIN. While only a maximum of 70 J kg^{-1} in CIN occurred in the 0000 UTC profiles, this could still inhibit cloud formation as the lack of turbulent fluxes at the surface would decrease mixing in the atmospheric boundary layer. Reduced boundary layer turbulence also decreases the available moisture from evaporation, further limiting the formation of low-level clouds[20,45]. The combination of upper-level drying and turbulent flux reduction during these clear-sky conditions highlights the importance of air-sea interactions and boundary layer processes during CBEs.

Unlike the gradual breakdown of the trades, the re-establishment of the trade winds is a rapid process. While surface winds and pressure gradients are weak over the GBR on March 10th (Fig. 9a), the trade winds have returned across the southern GBR in under one day as strong pressure gradients have extended up the east coast via coastal ridging (Fig. 9d). The ridging was likely enhanced by the mid-latitude cyclone residing in the Tasman Sea that combined with the anticyclone in the Great Australian Bight to accelerate strong southerlies up the east coast forcing the rapid return of the trade winds in a front-like wind shift[35,46,47]. Multiple weaker coastal ridging events occurred during the 2022 CBE, with the same pattern of a high-pressure system moving across the Great Australian Bight towards Tasmania (Fig. 8g). However, these events do not re-establish the trades winds over the GBR. The presence of COLs over eastern Australia during the heating period could suppress the equatorial extent of the ridging, preventing the re-establishment of the trade winds. However, the reason these other coastal ridging events do not extend towards the GBR requires further study.

Drivers of yearly variability

While repeated RWB events can be directly linked to the 2022 CBE, such events are a common summer-time feature across the east coast of Australia[41,43,48–50] and not all RWB events lead to a CBE. Looking beyond the connection to the mid-latitudes, we consider the potential influence of Madden-Julien Oscillation (MJO), Australian monsoon and El Niño Southern Oscillation (ENSO) during this event.

Throughout the summer, the active phase of the Australian monsoon produces extensive regions of cloud cover and heavy rainfall across northern Australia. Yet according to the Bureau of Meteorology[51] no monsoon bursts were reported during February or March 2022, which is consistent with the absence of widespread upper-level clouds in Fig. 7. The MJO was also inactive during February and March 2022[52], again consistent with the absence of wide-spread upper-level clouds. Possibly, a suppressed MJO and/or suppressed monsoon enhances the potential for ocean heating and a CBE given the reduction in upper-level cloud cover, but such an investigation is beyond the scope of this current research. We also note the absence of any tropical storms in the vicinity of the GBR over this period, which again can produce upper-level cloud cover.

Finally, we consider the influence of ENSO, where for many decades, correlations have been drawn between El Niño periods and mass CBEs globally[5,13,53]. El Niño is thought to drive GBR CBEs due to its association with reduced cloud cover and weakened trade winds over the Maritime Continent. Although in this study, the 2022 CBE is attributed to the overall trade wind breakdown and absence of cloud cover, it is noteworthy that these conditions occurred during a La Niña event, which is typically associated with increased cloud cover and strengthened trade winds. The periods of clear skies and weak/absent trade winds associated with GBR CBEs are not exclusive to El Niño periods[3,15,29,54]. Indeed, when considering the austral summer average, of the eight recent GBR CBEs, only two occurred under El Niño conditions (1998, 2016), with five during neutral conditions (2002, 2006, 2017, 2020 and 2024) and 2022 the sole La Niña event (Fig. 3c). As many studies have

highlighted the importance of local weather conditions during GBR CBEs[3,12,13,15,36,55] and have further shown GBR sea surface temperatures are more significantly correlated with local cloud cover than ENSO, especially in the shallow southern GBR[15]. The present study supports the idea that the changes in local weather conditions control the development of GBR CBEs, irrespective of the ENSO phase.

Climate change

The increasing frequency and intensity of CBEs due to climate change have been of high concern since the 1990s[53,54,56–59]. Five CBEs have occurred on the GBR since 2016 with a stark increase in intensity in the recent three events at our central GBR study site (Fig. 3). While at first glance the intensity of the 2022 CBE appears significantly higher than 2020, the cumulative intensity of the event's peak (>29.4 °C) are highly similar. The 2022 CBE was an extreme event on top of an anomalously warm summer, where December–January ocean temperatures were at the time the warmest on record[4]. More recently, February 2024 produced the highest on record ocean temperatures for the southern hemisphere[60]. Thus it is not surprising that an eighth mass GBR CBE was declared in early March 2024[61].

At Davies Reef from 1996–2022, the December–April daily average T_{4m} has increased by 0.48 °C. This warming has further increased to 0.63 °C when the analysis is extended to 2024. By simply removing the 0.48 °C increase, the severity of the 2022 CBE at Davies Reef decreases by 74% resulting in only 36 days exceeding the +1SD curve (10.2 °C degree heating days). Removing the 0.63 °C increase from the 2024 CBE decreases the intensity by 97% when using the +1SD threshold (0.47 °C degree heating days) with only one day exceeding the 29.4 °C threshold. A similar method was applied to the 2016 GBR CBE by Karnauskas[14], which potentially saw an increase of over 50% in intensity due to underlying ocean and air warming trends. These trends are consistent with the current warming under climate change over the GBR[59,62].

Conclusions

Using a combination of observations and reanalysis, this study shows the importance of the local and synoptic meteorology, in particular, the influence of the trade winds on ocean temperatures during the 2022 Great Barrier Reef (GBR) coral bleaching event (CBE) and marine heatwave (MHW). Using a daily-scale analysis highlights the trade winds impact on near-surface ocean temperatures through the response in the net surface energy budget. We find previously unreported connections between the local meteorology and synoptic patterns that influence that breakdown and re-establishment of the trades.

The key findings from this study are summarised below:

1. The trade winds are an important cooling mechanism for the GBR. The weakening and eventual breakdown of the trade winds initiates a period of ocean heating, allowing near-surface ocean temperatures to reach 30.5 °C at Davies Reef meeting MHW conditions. The sudden return to trade wind conditions rapidly cools the ocean by 1 °C in the first 48 h. The trade wind's ability to rapidly cool ocean temperatures over the shallow GBR suggests that a seasonal analysis may be limited, as seen for this 2022 CBE. Early heating in December had been erased by mid-February, before the onset of the heating that led to the CBE.
2. Fluctuations in Q_E are the primary driver of ocean heating and cooling for the 2022 CBE followed closely by Q_{SW}. As the trade winds collapse, periods of calm or northerly winds bringing high humidity combine to limit Q_E. During the cooling period, the re-establishment of the trades advects cool and dry air over the Reef, allowing Q_E to exceed 300 Wm^{-2}.
3. The mid-latitudes influence both the breakdown and return of the trade winds during the 2022 CBE. Repeated anticyclonic RWB and the development of associated COLs preceding and during the heating period is thought to drive the trade winds collapse. Coastal ridging then rapidly re-established stronger pressure gradients over the GBR allowing for the sudden return of the trade winds and rapid transition to ocean cooling conditions.
4. That the 2022 CBE formed under La Niña conditions highlights that the bleaching is controlled by the local meteorology, irrespective of the ENSO phase.
5. The 2022 GBR CBE was an extreme event on top of an anomalously warm summer. Nonetheless, like previous GBR CBEs, the 2022 and 2024 events at Davies Reef were potentially exacerbated by 74% and 97% respectively due to continued ocean temperature rise.
6. The 2022 case study highlights the interaction of extremes, as the same anticyclonic RWB and COL development associated with the 2022 Lismore flooding contributed to the reduction in cloud cover over the GBR. This study provides a detailed analysis of the meteorological drivers of the 2022 CBE, which is crucial for both our understanding of how GBR CBEs form and for the development of mitigation efforts and forecasting of future GBR CBEs. However, reliance on reanalysis fluxes provides limitations in the accuracy of the net surface energy budget which is crucial for unravelling the local meteorology's impact on ocean temperatures. This is also a single case study of one GBR site. Thus, further work is needed to understand the impacts and frequency of synoptic drivers, such as RWB, coastal ridging and non-trade wind conditions on GBR ocean temperatures in other CBEs. It is also important to note there may be considerable variability from one GBR CBE to another. Thus, RWB may not necessarily be relevant to other CBEs.

Data availability

All data sets used in this study are freely and publicly available online and may be accessed directly as follows. The Australian Institute of Marine Science Davies Reef data is available from their website (https://apps.aims.gov.au/metadata/view/5fc91100-4ade-11dc-8f56-00008a07204e). The ERA5 reanalysis data is available from the Copernicus Climate Data Store (https://cds.climate.copernicus.eu/cdsapp#!/search?type=dataset). The Himawari-8 full disk observational products are available from the NCI THREDDS data server (https://dapds00.

nci.org.au/thredds/catalogs/ra22/satellite-products/arc/obs/himawari-ahi/fldk/fldk.html) and the Himawari-8/AHI cloud mask is available from the NCI THREDDS data server (https://dapds00.nci.org.au/thredds/catalog/rv74/satellite-products/arc/der/himawari-ahi/cloud/cma/catalog.html). The Bureau of Meteorology SOI data is available from their website (http://www.bom.gov.au/climate/enso/soi/). The Townsville tidal data is available from the NCI THREDDS data server (https://thredds.nci.org.au/thredds/catalog/catalogs/fx31/publications/ANCHORS/ANCHORS.html).

Received: 5 July 2024; Accepted: 24 September 2024
Published online: 12 October 2024

References

1. Australian Institute of Marine Science (AIMS). Coral Bleaching Events (2024). https://www.aims.gov.au/research-topics/environmental-issues/coral-bleaching/coral-bleaching-events, last accessed: 13/05/2024.
2. Great Barrier Reef Marine Park Authority (GBRMPA), Australian Institute of Marine Science (AIMS), and Commonwealth Scientific and Industrial Research Organisation (CSIRO). Reef snapshot: Summer 2021-22 (Great Barrier Reef Marine Park Authority, 2022).
3. McGowan, H. & Theobald, A. Atypical weather patterns cause coral bleaching on the Great Barrier Reef, Australia during the 2021–2022 La Nina. *Sci. Rep.* **13**, 6397–6397. https://doi.org/10.1038/s41598-023-33613-1 (2023).
4. Spady, B. L. et al. Unprecedented early-summer heat stress and forecast of coral bleaching on the Great Barrier Reef, 2021–2022. *F1000Res* **11**, 127. https://doi.org/10.12688/f1000research.108724.4 (2022).
5. Glynn, P. W. Widespread coral mortality and the 1982–83 El Niño Warming Event. *Environ. Conserv.* **11**, 133–146. https://doi.org/10.1017/S0376892900013825 (1984).
6. Glynn, P. W. Coral reef bleaching: ecological perspectives. *Coral Reefs* **12**, 1–17. https://doi.org/10.1007/BF00303779 (1993).
7. Gleason, D. F. & Wellington, G. M. Ultraviolet radiation and coral bleaching. *Nature* **365**, 836–838. https://doi.org/10.1038/365836a0 (1993).
8. Glynn, P. W. Mass mortalities of echinoids and other reef flat organisms coincident with midday, low water exposures in Puerto Rico. *Mar. Biol.* **1**, 226–243. https://doi.org/10.1007/BF00347116 (1968).
9. Jokiel, P. L. & Brown, E. K. Global warming, regional trends and inshore environmental conditions influence coral bleaching in Hawaii. *Glob. Change Biol.* **10**, 1627–1641. https://doi.org/10.1111/j.1365-2486.2004.00836.x (2004).
10. Baird, A. H., Keith, S. A., Woolsey, E., Yoshida, R. & Naruse, T. Rapid coral mortality following unusually calm and hot conditions on Iriomote, Japan. *F1000Research* **6**. https://doi.org/10.12688/f1000research.12660.2 (2018).
11. Paparella, F., Xu, C., Vaughan, G. O. & Burt, J. A. Coral bleaching in the Persian/Arabian Gulf is modulated by summer winds. *Front. Mar. Sci.* **6**. https://doi.org/10.3389/fmars.2019.00205 (2019).
12. Skirving, W., Heron, M. & Heron, S. *The Hydrodynamics of a Bleaching Event: Implications for Management and Monitoring*, vol. 61, chap. 8, 145–161 (American Geophysical Union, 2006).
13. McGowan, H. & Theobald, A. ENSO Weather and Coral Bleaching on the Great Barrier Reef, Australia. *Geophys. Res. Lett.* **44**, 10601–10607. https://doi.org/10.1002/2017gl074877 (2017).
14. Karnauskas, K. B. Physical diagnosis of the 2016 Great Barrier Reef Bleaching Event. *Geophys. Res. Lett.* **47**. https://doi.org/10.1029/2019GL086177 (2020).
15. Zhao, W., Huang, Y., Siems, S. & Manton, M. The role of clouds in coral bleaching events over the Great Barrier Reef. *Geophys. Res. Lett.* **48**. https://doi.org/10.1029/2021GL093936 (2021).
16. Bainbridge, S. J. Temperature and light patterns at four reefs along the Great Barrier Reef during the 2015–2016 austral summer: understanding patterns of observed coral bleaching. *J. Oper. Oceanogr.* **10**, 16–29. https://doi.org/10.1080/1755876X.2017.1290863 (2017).
17. MacKellar, M. C., McGowan, H. A. & Phinn, S. R. An observational heat budget analysis of a coral reef, Heron Reef, Great Barrier Reef, Australia. *J. Geophys. Res. Atmos.* **118**, 2547–2559. https://doi.org/10.1002/jgrd.50270 (2013).
18. Talley, L., Pickard, G., Emery, W. & Swift, J. *Mass, Salt, and Heat Budgets and Wind Forcing*, chap. 5 (2011).
19. Fordyce, A. J., Ainsworth, T. D., Heron, S. F. & Leggat, W. Marine heatwave hotspots in coral reef environments: physical drivers, ecophysiological outcomes, and impact upon structural complexity. *Front. Mar. Sci.* **6**. https://doi.org/10.3389/fmars.2019.00498 (2019).
20. Malkus, J. S. On the structure of the trade wind moist layer. *Physical Oceanography and Meteorology* (1958).
21. Connor, G. J. & Bonell, M. Air mass and dynamic parameters affecting trade wind precipitation on the northeast Queensland tropical coast. *Int. J. Climatol.* **18**, 1357–1372. (1998).
22. Zhao, W., Huang, Y., Siems, S., Manton, M. & Harrison, D. Interactions between trade wind clouds and local forcings over the Great Barrier Reef: a case study using convection-permitting simulations. *Atmos. Chem. Phys.* **24**, 5713–5736. https://doi.org/10.5194/acp-24-5713-2024 (2024).
23. Pope, M., Jakob, C. & Reeder, M. J. Regimes of the North Australian wet season. *J. Clim.* **22**, 6699–6715. https://doi.org/10.1175/2009jcli3057.1 (2009).
24. Murphy, M. J., Siems, S. T. & Manton, M. J. Regional variation in the wet season of northern Australia. *Mon. Weather Rev.* **144**, 4941–4962. https://doi.org/10.1175/MWR-D-16-0133.1 (2016).
25. Hobday, A. J. et al. A hierarchical approach to defining marine heatwaves. *Prog. Oceanogr.* **141**, 227–238. https://doi.org/10.1016/j.pocean.2015.12.014 (2016).
26. Bureau of Meteorology (BOM). Special Climate Report 76—Extreme rainfall and flooding in south-eastern Queensland and eastern New South Wales (2022).
27. Hague, B. S. et al. ANCHORS: A multi-decadal tide gauge dataset to monitor Australian relative sea level changes. *Geosci. Data J.* **9**, 256–272. https://doi.org/10.1002/gdj3.136 (2021).
28. Hersbach, H. et al. The era5 global reanalysis. *Q. J. R. Meteorol. Soc.* **146**, 1999–2049. https://doi.org/10.1002/qj.3803 (2020).
29. Benthuysen, J. A., Smith, G. A., Spillman, C. M. & Steinberg, C. R. Subseasonal prediction of the 2020 Great Barrier Reef and Coral Sea marine heatwave. *Environ. Res. Lett* **16**, 124050. https://doi.org/10.1088/1748-9326/ac3aa1 (2021).
30. Berkelmans, R. Time-integrated thermal bleaching thresholds of reefs and their variation on the Great Barrier Reef. *Mar. Ecol. Prog. Ser. (Halstenbek)* **229**, 73–82. https://doi.org/10.3354/meps229073 (2002).
31. Glynn, P. W. & D'Croz, L. Experimental evidence for high temperature stress as the cause of El Nino-coincident coral mortality. *Coral Reefs* **8**, 181–191 (1990).
32. Liu, G., Strong, A. E. & Skirving, W. Remote sensing of sea surface temperatures during 2002 Barrier Reef coral bleaching. *Eos Trans. Am. Geophys. Union* **84**, 137–141. https://doi.org/10.1029/2003eo150001 (2003).
33. Nuijens, L., Stevens, B. & Siebesma, A. P. The environment of precipitating shallow cumulus convection. *J. Atmos. Sci.* **66**, 1962–1979. https://doi.org/10.1175/2008jas2841.1 (2009).
34. Mcintyre, M. E. & Palmer, T. N. Breaking planetary waves in the stratosphere. *Nature* **305**, 593–600. https://doi.org/10.1038/305593a0 (1983).

35. Holland, G. J. & Leslie, L. M. Ducted coastal ridging over S.E. Australia. *Q. J. R. Meteorol. Soc.* **112**, 731–748. https://doi.org/10.1002/qj.49711247310 (1986).
36. MacKellar, M. C. & McGowan, H. A. Air-sea energy exchanges measured by eddy covariance during a localised coral bleaching event, Heron Reef, Great Barrier Reef, Australia. *Geophys. Res. Lett.* **37**. https://doi.org/10.1029/2010gl045291 (2010).
37. Abir, S., McGowan, H. A., Shaked, Y. & Lensky, N. G. Identifying an evaporative thermal refugium for the preservation of coral reefs in a warming world–The Gulf of Eilat (Aqaba). *J. Geophys. Res. Atmos.* **127**. https://doi.org/10.1029/2022jd036845 (2022).
38. Burt, J. A., Paparella, F., Al-Mansoori, N., Al-Mansoori, A. & Al-Jailani, H. Causes and consequences of the 2017 coral bleaching event in the southern Persian/Arabian Gulf. *Coral Reefs* **38**, 567–589. https://doi.org/10.1007/s00338-019-01767-y (2019).
39. West, J. M. & Salm, R. V. Resistance and resilience to coral bleaching: implications for coral reef conservation and management. *Conserv. Biol.* **17**, 956–967. https://doi.org/10.1046/j.1523-1739.2003.02055.x (2003).
40. Hoskins, B. J., McIntyre, M. E. & Robertson, A. W. On the use and significance of isentropic potential vorticity maps. *Q. J. R. Meteorol. Soc.* **111**, 877–946. https://doi.org/10.1002/qj.49711147002 (1985).
41. Robinson, C. M., Barnes, M. A., Narsey, S. & Reeder, M. J. The meteorology of the. North Queensland floods. *Q. J. R. Meteorol. Soc.* **2024**. https://doi.org/10.1002/qj.4685 (2019).
42. Ndarana, T. & Waugh, D. W. The link between cut-off lows and Rossby wave breaking in the Southern Hemisphere. *Q. J. R. Meteorol. Soc.* **136**, 869–885. https://doi.org/10.1002/qj.627 (2010).
43. Barnes, M. A., King, M., Reeder, M. & Jakob, C. The dynamics of slow-moving coherent cyclonic potential vorticity anomalies and their links to heavy rainfall over the eastern seaboard of Australia. *Q. J. R. Meteorol. Soc.* **149**, 2233–2251. https://doi.org/10.1002/qj.4503 (2023).
44. Aemisegger, F. et al. How Rossby wave breaking modulates the water cycle in the North Atlantic trade wind region. *Weather Clim. Dyn.* **2**, 281–309. https://doi.org/10.5194/wcd-2-281-2021 (2021).
45. Ren, Y., Fu, S. & Xue, H. The sensitivity of a mid-latitude maritime stratocumulus cloud to surface fluxes. *Atmos. Res.* **293**. https://doi.org/10.1016/j.atmosres.2023.106912 (2023).
46. Baines, P. G. The dynamics of the southerly buster. *Aust. Meteorol. Mag.* **28**, 175–200 (1980).
47. Speer, M. S. & Leslie, L. M. A climatology of coastal ridging over south-eastern Australia. *Int. J. Climatol.* **17**, 831–845. (1997).
48. Berry, G. J., Reeder, M. J. & Jakob, C. Coherent synoptic disturbances in the Australian monsoon. *J. Clim.* **25**, 8409–8421. https://doi.org/10.1175/jcli-d-12-00143.1 (2012).
49. O'Brien, L. & Reeder, M. J. Southern Hemisphere summertime Rossby waves and weather in the Australian region. *Q. J. R. Meteorol. Soc.* **143**, 2374–2388. https://doi.org/10.1002/qj.3090 (2017).
50. Ali, S. M., Röthlisberger, M., Parker, T., Kornhuber, K. & Martius, O. Recurrent Rossby waves and south-eastern Australian heatwaves. *Weather Clim. Dyn.* **3**, 1139–1156. https://doi.org/10.5194/wcd-3-1139-2022 (2022).
51. Bureau of Meteorology (BOM). Australia's 2021–22 northern wet season (2022). http://www.bom.gov.au/climate/current/season/tropics/archive/202204.summary.shtml, last accessed: 28/03/2024.
52. Bureau of Meteorology (BOM). MJO monitoring (2022). http://www.bom.gov.au/climate/mjo/, last accessed: 28/03/2024.
53. Baker, A. C., Glynn, P. W. & Riegl, B. Climate change and coral reef bleaching: An ecological assessment of long-term impacts, recovery trends and future outlook. *Estuar. Coast. Shelf Sci.* **80**, 435–471. https://doi.org/10.1016/j.ecss.2008.09.003 (2008).
54. Hughes, T. P. et al. Spatial and temporal patterns of mass bleaching of corals in the Anthropocene. *Science* **359**, 80–83. https://doi.org/10.1126/science.aan8048 (2018).
55. Redondo-Rodriguez, A., Weeks, S. J., Berkelmans, R., Hoegh-Guldberg, O. & Lough, J. M. Climate variability of the Great Barrier Reef in relation to the tropical Pacific and El Nino-Southern Oscillation. *Mar. Freshw. Res.* **63**, 34–47. https://doi.org/10.1071/MF11151 (2012).
56. Glynn, P. W. Coral reef bleaching: Facts, hypotheses and implications. *Glob. Change Biol.* **2**, 495–509. https://doi.org/10.1111/j.1365-2486.1996.tb00063.x (1996).
57. Hoegh-Guldberg, O. Climate change, coral bleaching and the future of the world's coral reefs. *Mar. Freshw. Res.* **50**, 839–866. https://doi.org/10.1071/MF99078 (1999).
58. Hughes, T. P. et al. Global warming and recurrent mass bleaching of corals. *Nature* **543**, 373–377. https://doi.org/10.1038/nature21707 (2017).
59. Henley, B. J. et al. Highest ocean heat in four centuries places Great Barrier Reef in danger. *Nature* **632**, 320–326. https://doi.org/10.1038/s41586-024-07672-x (2024).
60. National Oceanic and Atmospheric Administration (NOAA). February 2024 Global Climate Report (2024). https://www.ncei.noaa.gov/access/monitoring/monthly-report/global/202402, last accessed: 27/03/2024.
61. Australian Institute of Marine Science (AIMS). Aerial surveys reveal mass coral bleaching event unfolding on the Great Barrier Reef (2024). https://www.aims.gov.au/information-centre/news-and-stories/aerial-surveys-reveal-mass-coral-bleaching-event-unfolding-great-barrier-reef, last accessed: 27/03/2024.
62. Heron, S. F., Maynard, J. A., van Hooidonk, R. & Eakin, C. M. Warming Trends and Bleaching Stress of the World's Coral Reefs 1985–2012. *Sci. Rep.* **6**, 38402. https://doi.org/10.1038/srep38402 (2016).

Acknowledgements

This work was supported by the Reef Restoration and Adaptation Program. The Reef Restoration and Adaptation Program is funded by the partnership between the Australian Governments Reef Trust and the Great Barrier Reef Foundation. The authors would like to acknowledge the Traditional Owners of the Great Barrier Reef, particularly the Wulgurukaba and Bindal people of the Townsville region near the area of our case study. This research is also supported by the ARC Centre of Excellence for Climate Extremes (grant no. CE170100023). We acknowledge the National Computational Infrastructure for their provision of computational resources and services. Yi Huang and Steve Siems are further supported by an Australian Research Council Discovery Grant (grant no. DP230100639).

Author contributions

L.S.R, S.T.S, Y.H., M.J.M. and M.J.R. conceived the original ideas for the study. L.S.R. and W.Z. collected the data. L.S.R. performed the analysis and prepared the draft manuscript. S.T.S., Y.H., W.Z., D.P.H. and M.J.R supervised and reviewed the manuscript.

Declarations

Competing interests

The authors declare no competing interests.

Additional information

Correspondence and requests for materials should be addressed to L.S.R.

Reprints and permissions information is available at www.nature.com/reprints.

Publisher's note Springer Nature remains neutral with regard to jurisdictional claims in published maps and institutional affiliations.